Absolute–convective instabilities and their associated wave packets in a compressible reacting mixing layer

F. Q. Hu, T. L. Jackson, and D. G. Lasseigne
Department of Mathematics and Statistics, Old Dominion University, Norfolk, Virginia 23529

C. E. Grosch
Department of Oceanography and Department of Computer Science, Old Dominion University, Norfolk, Virginia 23529

(Received 2 April 1992; accepted 17 November 1992)

In this paper the transition from convective to absolute instability in a reacting compressible mixing layer with finite rate chemistry is examined. The reaction is assumed to be one step, irreversible, and of Arrhenius type. It is shown that absolute instability can exist for moderate heat release without backflow. The effects of the temperature ratio, heat release parameter, Zeldovich number, equivalence ratio, direction of propagation of the disturbances, and the Mach number on the transition value of the velocity ratio are given. The present results are compared to those obtained from the flame sheet model for the temperature using the Lock similarity solution for the velocity profile. Finally, the structure of the wave packets produced by an impulse in the absolutely unstable flow is examined.

I. INTRODUCTION

Understanding the stability characteristics of reacting compressible free shear flows is of fundamental importance (Jackson[1]) and may have possible usefulness in the development of the scramjet engine (Beach[2]). As discussed by Drummond and Mukunda,[3] the scramjet combustor flow is complex but spatially developing and reacting compressible mixing layers of fuel and oxidizer provide the simplest relevant model. Mixing of the two gases takes place in the shear layer and combustion occurs when there is both sufficient fuel and oxidizer present at the same point. The residence time of the fuel and air in the combustion chamber can be very short; therefore, it is extremely important that a high mixing rate of the fuel and oxidizer be achieved so that complete combustion is attained before the fuel is convected out of the engine. Compounding the problem of a very short residence time is that the mixing rates of shear layers have been shown experimentally to decrease as the Mach number increases from zero (e.g., Brown and Roshko;[4] Chinzei *et al.*;[5] Papamoschou and Roshko;[6,7] and Clemens[8]). As a result, a major theme of current research is mixing enhancement techniques. One obvious mixing enhancement technique is to force the shear layer at some prescribed frequency, usually computed from linear stability analysis. It is essential to determine whether reacting flows are convectively or absolutely unstable if one wishes to control the downstream evolution of the flow. An absolutely unstable flow is not sensitive to external disturbances and initial conditions; thus, experiments may not be completely reproducible nor may "flow management" techniques such as forcing be useful. In this paper, we address the question of transition from convective to absolute instability in compressible reacting shear flows and compute the associated wave packets to investigate their time evolution.

The concept of absolute and convective instabilities was introduced by Briggs[9] in the context of plasma instability. The same idea was put forward independently by Gaster[10,11] within the context of classical hydrodynamic stability theory based on the Orr–Sommerfeld equation. A flow is said to be absolutely unstable if the response to an impulse in space and time is unbounded everywhere in space for large time. On the other hand, if the response to an impulse is a wave packet propagating downstream from the source with the waves forming the packet having growing amplitudes, the flow is said to be convectively unstable. With this type of instability, the response decays to zero everywhere in space for large enough time. These concepts have been applied to classify the instabilities of both incompressible and compressible flows; see, for example, the review article by Huerre and Monkewitz.[12] In particular, nonreacting subsonic compressible mixing layers (Huerre and Monkewitz;[13] Pavithran and Redekopp;[14] and Jackson and Grosch[15]) have been found to be convectively unstable unless there is an appreciable amount of backflow.

In the course of a comprehensive study of the stability of a reacting compressible mixing layer using a hyperbolic tangent for the mean velocity profile and a flame sheet model to describe the reaction, Jackson and Grosch[16] found that the flow switches from convective to absolute instability with a sufficient amount of heat release even without any reversed flow. Since piecewise continuous profiles, such as the temperature of the flame sheet model, can give spurious results, it is desirable (i) to reexamine the question of absolute/convective instability for reacting flows with finite rate chemistry and (ii) to compare the results with those found using a flame sheet model.

The ignition and structure of a reacting compressible mixing layer using finite rate chemistry has been studied recently by Grosch and Jackson.[17] They solved the partial differential equations for the velocity, temperature, and mass fractions with appropriate initial and boundary conditions by, in the first instance, marching downstream without making any assumptions as to similarity. They

 0899-8213/93/040901-15$06.00 © 1993 American Institute of Physics

Reuse of AIP Publishing content is subject to the terms at: https://publishing.aip.org/authors/rights-and-permissions. Download to IP: 128.82.15.135 On: Sun, 28 Aug 2016 19:44:02

found that the velocity field attained a self-similar form at a very small downstream position. This was in the region where ignition had not occurred and the temperature and mass fractions were determined by chemically frozen diffusion equations. Because of this, they transformed the equations to the self-similar form and used the self-similar velocity, temperature, and mass fraction profiles as the initial conditions of the problem. Of course the temperature and mass fraction profiles evolved further with downstream distance from this initial point and the three regimes of ignition, deflagration, and a diffusion flame were found to occur. The diffusion flame continued to evolve farther downstream and very far downstream of the ignition point the diffusion flame finally evolved to a flame sheet. In this paper we follow Grosch and Jackson and use the chemically frozen similarity profiles as the initial conditions for the downstream marching solution of the mean flow equations.

An important consideration in this, and any other study of reacting flow, is the representation of chemistry of the reaction. The flame sheet is the simplest possible model. If the chemistry is assumed to have a finite rate, a wide variety of models have been used. These range from a detailed representation of the reactions using multiple rate equations and including intermediate species[3] to a one-step irreversible reaction.[17] The former model is believed to give a very accurate representation of the details of the chemistry but requires extremely expensive and time consuming numerical calculations. The latter model is widely used in combustion studies and is believed to at least model some aspects of the relevant chemistry. It has a nonlinear dependence on temperature and mass fractions but is simple enough that the analysis and numerics are tractable. Because our primary interest [items (i) and (ii) above] is to find the effect of finite rate chemistry, in comparison to the flame sheet, on the convective/absolute transition we chose to use the simplest finite rate reaction model: the one-step irreversible Arrhenius model. We believe that this model will give correct qualitative results but we expect that there will be quantitative differences with the results of calculations using the more detailed rate equation models.

In any compressible flow calculations it is necessary to specify the property variations with temperature and pressure and the appropriate form of the equation of state. At sufficiently high temperature and/or low density it will be necessary to use an equation of state incorporating real gas effects.[18] However, in this study the Mach numbers are moderate and we will assume that a perfect gas law is valid. We have examined the effect of the form of the velocity profile, the value of the Prandtl number, and the viscosity–temperature relation on the stability characteristics of the nonreacting compressible mixing layer.[19] It was found that the *qualitative behavior* of the solutions was independent of these variations although there were quantitative differences in the growth rates and phase speeds. In view of the fact that we are using a simplified combustion model in these calculations, we can only expect that our results will show correct qualitative dependency of the convective/absolute instability transition on the flow parameters.

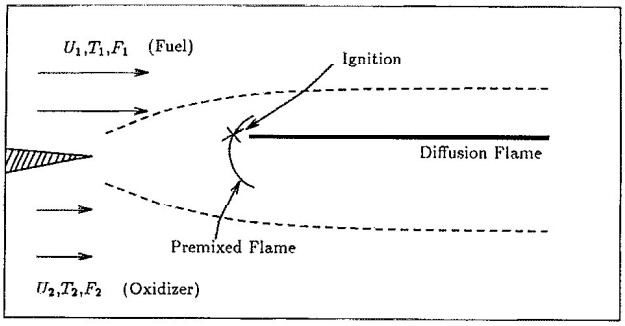

FIG. 1. Schematic showing the reacting mixing layer.

Therefore we have chosen to use simple property variations: the Prandtl number constant and equal to one and a linear variation of the viscosity coefficient with temperature.

The finite rate model involves solving the Lock similarity profile for the velocities, together with the temperature and mass fraction equations using a one-step irreversible reaction of Arrhenius type. For consistency, the flame sheet model must also involve solving the Lock similarity profile for the velocities, assuming an infinite rate reaction, and using a Crocco relation for the temperature and mass fractions on either side of the flame sheet. We have done this for the flame sheet calculations reported here. This is in contrast to our previous reported results using the flame sheet[16] where we approximated the velocity profile by a hyperbolic tangent.

In Sec. II, a brief review of the formulation of the mean flow equations is given for completeness. In Sec. III, the inviscid three-dimensional stability equations including the effect of finite rate chemistry are derived. Certain results pertaining to the linear stability of this flow with finite rate chemistry and comparisons to the results obtained with the flame sheet model are given in Sec. IV. Section V contains results on the transition from convective to absolute instability using the finite rate chemistry model, which are then compared with those obtained from the flame sheet model. The flame sheet model is found to provide excellent predictions on the transition values provided one is downstream of ignition and Zeldovich numbers are greater than about 10. Therefore, in Sec. VI results of calculations of wave packets using the flame sheet model in cases of both convective and absolute instability are given. Finally, Sec. VII contains our conclusions.

II. FORMULATION OF THE MEAN FLOW EQUATIONS

The nondimensional equations governing the steady two-dimensional flow of a compressible, reacting mixing layer with zero pressure gradient lying between streams of fuel and oxidizer with different speeds and temperatures (Fig. 1) are given by

$$(\rho U)_x+(\rho V)_y=0, \tag{1a}$$

$$1=\rho T, \tag{1b}$$

Reuse of AIP Publishing content is subject to the terms at: https://publishing.aip.org/authors/rights-and-permissions. Download to IP: 128.82.15.135 On: Sun, 28 Aug 2016 19:44:02

$$\rho(UU_x+VU_y)=(\mu U_y)_y, \tag{1c}$$

$$\rho(UT_x+VT_y)=\mathrm{Pr}^{-1}(\mu T_y)_y+(\gamma-1)M^2\mu U_y^2+\beta\Omega, \tag{1d}$$

$$\rho(UF_{j,x}+VF_{j,y})=\mathrm{Sc}_j^{-1}(\mu F_{j,y})_y-\beta_j\Omega, \quad j=1,2, \tag{1e}$$

$$\Omega=D\rho F_1F_2e^{-\mathrm{Ze}/T}. \tag{1f}$$

In these equations, the x axis is along the direction of flow, the y axis is normal to the flow, U and V are the velocity components in the x and y directions, respectively; ρ is the density; T is the temperature; and F_1 and F_2 are the mass fractions of the fuel and oxidizer, respectively. The reaction is assumed to be one step, irreversible, and of Arrhenius type. The viscosity μ is assumed to be a function of temperature. The nondimensional parameters appearing above are the Prandtl number Pr, the Schmidt number $\mathrm{Sc}_j=\mathrm{Pr}\,\mathrm{Le}_j$ for species j where Le_j is the Lewis number for species j, the parameters β_j involve stoichiometry of the reaction and are taken to be one, the Mach number is $M=U_\infty/a_\infty$, the Zeldovich number is $\mathrm{Ze}=E/R\,T_\infty$ with E the dimensional activation energy and R the universal gas constant, the Damköhler number is D defined as the ratio of the characteristic diffusion time scale to the characteristic chemical time scale, β is the heat release per unit mass fraction of the fuel, and finally γ is the specific-heats ratio. The equations have been nondimensionalized by the free-stream values T_∞, ρ_∞, U_∞, $F_{1,\infty}$ for the temperature, density, velocities, and mass fractions, respectively, and lengths have been referred to some characteristic length scale of the flow. The boundary conditions consistent with (1) are

$$T=U=F_1=1, \quad F_2=0$$

$$\text{at } x=0,\ y>0 \text{ and } x>0,\ y\to\infty, \tag{2a}$$

$$T=\beta_T,\ U=\beta_U<1,\ F_1=0,\ F_2=\phi^{-1}$$

$$\text{at } x=0,\ y<0 \text{ and } x>0,\ y\to-\infty, \tag{2b}$$

where $\phi=F_{1,\infty}/F_{2,-\infty}$ is the equivalence ratio defined as the ratio of the mass fraction F_1 of the fuel to the mass fraction F_2 of the oxidizer. If $\phi=1$, the mixture is stoichiometric; if $\phi>1$, it is fuel rich, while if $\phi<1$, it is fuel lean.

The mean flow equations (1) are first transformed into the incompressible form by means of the Howarth–Dorodnitzyn transformation

$$Y=\int_0^y \rho\,dy, \quad \hat{V}=\rho V+U\int_0^y \rho_x\,dy, \tag{3}$$

and then to the similarity variable for the chemically frozen heat conduction problem,

$$\eta=Y/2\sqrt{x}. \tag{4}$$

Under these transformations, with $U=f'(\eta)$ and $\hat{V}=(\eta f'-f)/x$, Eq. (1) becomes

$$f'''+2ff''=0, \tag{5a}$$

$$4xf'T_x-\mathrm{Pr}^{-1}T''-2fT'-(\gamma-1)M^2(f'')^2=4x\beta DF_1F_2e^{-\mathrm{Ze}/T}, \tag{5b}$$

$$4xf'F_{j,x}-\mathrm{Sc}_j^{-1}F_j''-2fF_j'=-4xDF_1F_2e^{-\mathrm{Ze}/T}, \tag{5c}$$

where the primes indicate partial differentiation with respect to the similarity variable η, and where the linear viscosity law $\mu=T$ has been assumed (for Chapman's linear law $\mu=CT$, the constant C can be scaled out by rescaling η and f appropriately, but must be borne in mind when transforming the variables back to their dimensional forms). In terms of the transformed variables, the boundary conditions are

$$T=f'=F_1=1,\ F_2=0$$

$$\text{at } x=0,\ \eta>0 \text{ and } x>0,\ \eta\to\infty, \tag{6a}$$

$$T=\beta_T,\ f'=\beta_U,\ F_1=0,\ F_2=\phi^{-1}$$

$$\text{at } x=0,\ \eta<0 \text{ and } x>0,\ \eta\to-\infty. \tag{6b}$$

In all of the calculations, we have taken $0\leqslant\beta_U<1$ as there is no solution of (5a) with reversed flow. We also note that the Damköhler number D can be scaled out of the equations by a rescaling of the x coordinate. However, rescaling x by the Damköhler number is not particularly useful since D is typically exponentially large and the rescaled coordinate would be exponentially stretched, which is not desirable from a numerical viewpoint. Finally, rescaling to eliminate the Damköhler number is only appropriate for the boundary-layer equations and is not possible when solving the full Navier–Stokes equations (see, for example, Ghoniem and Heidarinejad[20]).

In this paper the results of stability calculations carried out for the above flow field over a range of downstream positions are presented. The mean profiles are found by numerically integrating (5) with the initial and boundary conditions given by (6). For the comparisons to be made between the finite rate model and the flame sheet model, the same stability calculations are carried out using the Lock similarity solution for the velocity field [Eq. (5a)] and the flame sheet model for the temperature and mass fraction fields. For completeness, the equations for the temperature and mass fractions for the flame sheet approximation are given below.

For finite Damköhler number a thin diffusion flame exists within the mixing layer and is characterized by near-equilibrium conditions: $F_1=0$ on one side of the flame and $F_2=0$ on the other. In the limit of infinite Damköhler number this thin diffusion flame reduces to a flame sheet described by

$$F_1=1-(1+\phi^{-1})\left(\frac{1-U}{1-\beta_U}\right), \quad F_2=0, \tag{7a}$$

$$T=\beta_T+\beta\phi^{-1}+(1-\beta_T-\beta\phi^{-1})\left(\frac{U-\beta_U}{1-\beta_U}\right)+\frac{\gamma-1}{2}M^2(U-\beta_U)(1-U), \tag{7b}$$

for $\eta>\eta_f$, and

Reuse of AIP Publishing content is subject to the terms at: https://publishing.aip.org/authors/rights-and-permissions. Download to IP: 128.82.15.135 On: Sun, 28 Aug 2016 19:44:02

$$F_1=0, \quad F_2=\phi^{-1}-(1+\phi^{-1})\left(\frac{U-\beta_U}{1-\beta_U}\right), \tag{8a}$$

$$T=\beta_T+(1-\beta_T+\beta)\left(\frac{U-\beta_U}{1-\beta_U}\right)+\frac{\gamma-1}{2}M^2(U-\beta_U)(1-U), \tag{8b}$$

for $\eta<\eta_f$, where η_f is the location of the flame sheet given by the implicit relation

$$U_f\equiv U(\eta_f)=\frac{1+\beta_U\phi}{1+\phi}. \tag{9}$$

Both reactants vanish at η_f, and T takes the adiabatic flame value

$$T_f=\beta_T+(1-\beta_T+\beta)\left(\frac{U_f-\beta_U}{1-\beta_U}\right)+\frac{\gamma-1}{2}M^2(U_f-\beta_U)(1-U_f). \tag{10}$$

The implicit relation for the flame location is independent of β_T and M. This is only the case for a linear viscosity law where the momentum equation decouples from the energy equation. For a more general viscosity law, the implicit relation for the flame location depends on β_T and M as well. Independently of the viscosity–temperature relation, when using (3) and (4) to transform back to the physical coordinates the diffusion flame location depends on all four parameters: β_U, ϕ, β_T, and M.

III. DERIVATION OF THE STABILITY EQUATIONS

The derivation of the equations governing the stability of the reacting flow is straightforward except for the treatment of the source term. In a previous study of the stability of a reacting compressible mixing layer (Jackson and Grosch[16]), the limit of infinite Damköhler number was taken thus reducing the combustion zone to a flame sheet. In the flame sheet limit the perturbation does not affect the heat release in the sheet, it merely wrinkles the sheet. Therefore, the only effect the reaction has on the flow stability is through the change in the mean temperature distribution from that of the nonreacting flow. With finite rate chemistry, the perturbations not only wrinkle the combustion zone but also change the rate of heat release in the reaction. This, in turn, affects the stability of the flow.

As we are considering the three-dimensional inviscid stability problem, the governing equations are

$$P=\rho T, \tag{11a}$$

$$\rho_t+(\rho u)_x+(\rho v)_y+(\rho w)_z=0, \tag{11b}$$

$$\rho(u_t+uu_x+vu_y+wu_z)+\frac{1}{\gamma M^2}P_x=0, \tag{11c}$$

$$\rho(v_t+uv_x+vv_y+wv_z)+\frac{1}{\gamma M^2}P_y=0, \tag{11d}$$

$$\rho(w_t+uw_x+vw_y+ww_z)+\frac{1}{\gamma M^2}P_z=0, \tag{11e}$$

$$\rho(T_t+uT_x+vT_y+wT_z)-\frac{\gamma-1}{\gamma}(P_t+uP_x+vP_y+wP_z)=\beta\Omega, \tag{11f}$$

$$\rho(F_{j,t}+uF_{j,x}+vF_{j,y}+wF_{j,z})=-\Omega, \quad j=1,2, \tag{11g}$$

with Ω given by (1f). The mass fractions F_j can be replaced by the quantities $H_j=T+\beta F_j$, which satisfy equations without the source terms. The flow is perturbed with wave disturbances of the form

$$[u,v,w,P,\rho,T,H_j,F_j](x,y,t)=[U,0,0,1,\rho,T,H_j,F_j](y)+\epsilon[\hat{u},\alpha\cos\theta\hat{v},\hat{w},\Pi,\hat{\rho},\hat{T},\hat{H}_j,\hat{F}_j]\times(y)e^{i[\alpha(x\cos\theta+z\sin\theta)-\omega t]}, \tag{12}$$

where $\epsilon\ll 1$, α is the wave number, θ is the direction of propagation in the x-z plane, and ω is the frequency. For spatial theory, ω is required to be real and solutions are sought for which α is complex. For temporal theory, α is assumed to be real and solutions are sought for which ω is complex. The amplification rates of the disturbances are then given by $-\alpha_i$ or ω_i, respectively. The disturbances are two dimensional for $\theta=0°$ and otherwise oblique.

Upon carrying out the transformations from y to Y and then to η, it is straightforward to show that

$$\hat{T}+\beta\hat{F}_j=\hat{H}_j=\frac{\gamma-1}{\gamma}T\Pi-\frac{H_j'\Pi'}{\gamma M^2\alpha^2\cos^2\theta T(U-c)^2}, \tag{13}$$

where primes indicate differentiation with respect to η, α and ω have been rescaled by $\sqrt{x}$, and $c=\omega/\alpha\cos\theta$ is the complex phase speed. The source term Ω, expanded to order ϵ is

$$\Omega(F_1+\epsilon\hat{F}_1,F_2+\epsilon\hat{F}_2,T_1+\epsilon\hat{T})=\Omega(F_1,F_2,T)+\epsilon\left(\frac{\partial\Omega}{\partial F_1}\hat{F}_1+\frac{\partial\Omega}{\partial F_2}\hat{F}_2+\frac{\partial\Omega}{\partial T}\hat{T}\right). \tag{14}$$

Using (13) and the relation

$$\Pi'+i\gamma M^2\alpha^2\cos^2\theta(U-c)\hat{v}=0 \tag{15}$$

found from (11d), the order ϵ term for the quantity $\beta\Omega$ becomes

$$\frac{\gamma-1}{\gamma}T(Q_1+Q_2)\Pi-\frac{Q_1H_1'+Q_2H_2'}{\gamma M^2\alpha^2\cos^2\theta(U-c)^2}\Pi'+(\beta Q_3-Q_1-Q_2)\hat{T}, \tag{16}$$

with

$$Q_1=\frac{\partial\Omega}{\partial F_1}, \quad Q_2=\frac{\partial\Omega}{\partial F_2}, \quad Q_3=\frac{\partial\Omega}{\partial T}. \tag{17}$$

The equation for the pressure perturbation, found by utilizing (11a)–(11c), (11e), (11f), and (16), is

Reuse of AIP Publishing content is subject to the terms at: https://publishing.aip.org/authors/rights-and-permissions. Download to IP: 128.82.15.135 On: Sun, 28 Aug 2016 19:44:02

$$\Pi''-\left(\frac{2U'}{U-c}+(1-K_1)\frac{T'}{T}\right)\Pi'$$
$$-\alpha^2 T[T-K_2 M^2\cos^2\theta(U-c)^2]\Pi=0, \tag{18}$$

where

$$K_1=J_3/J_1, \quad K_2=\gamma-(\gamma-1)(J_2/J_1) \tag{19}$$

and

$$J_1=1+i\frac{(\beta Q_3-Q_1-Q_2)T}{\alpha\cos\theta(U-c)}, \tag{20}$$

$$J_2=1-i\frac{(Q_1+Q_2)T}{\alpha\cos\theta(U-c)}, \tag{21}$$

$$J_3=1-i\frac{(Q_1H_1'+Q_2H_2')T}{\alpha\cos\theta T'(U-c)}. \tag{22}$$

The appropriate boundary conditions for Π are obtained by considering the limiting form of (18) as $\eta\to\pm\infty$ which gives that

$$\Pi\to\exp(\pm\Delta_\pm\eta), \tag{23}$$

where

$$\Delta_+^2=\alpha^2[1-M^2\cos^2\theta(1-c)^2],$$
$$\Delta_-^2=\alpha^2\beta_T[\beta_T-M^2\cos^2\theta(\beta_U-c)^2]. \tag{24}$$

The values of the phase speed for which $\Delta_\pm^2$ vanishes are

$$c_+=1-\frac{1}{M\cos\theta}, \quad c_-=\beta_U+\frac{\sqrt{\beta_T}}{M\cos\theta}, \tag{25}$$

where c_+ is the phase speed of a sonic disturbance in the fast stream and c_- is the phase speed of a sonic disturbance in the slow stream. When

$$M\cos\theta=M_*\equiv\frac{1+\sqrt{\beta_T}}{1-\beta_U}, \tag{26}$$

$c_\pm$ are equal.

The nature of the disturbances and the appropriate boundary conditions are illustrated by reference to Fig. 1 of Jackson and Grosch,[21] which is a plot of $c_\pm$ vs M for a typical value of β_T and β_U, the nondimensional temperature and speed at $-\infty$, respectively, and for $\theta=0°$. These curves divide the phase-speed–Mach-number plane into four regions. If a neutral disturbance exists with a Mach number and phase speed in region 1, it is subsonic at both boundaries, and is classified as a subsonic neutral mode. In region 3, the neutral disturbance is supersonic at both boundaries, and is classified as a supersonic–supersonic neutral mode. In region 2, the neutral disturbance is subsonic in the fast stream and supersonic in the slow stream, and is classified as a fast neutral mode. Finally, in region 4, the neutral disturbance is supersonic in the fast stream and subsonic in the slow stream, and is classified as a slow neutral mode. For oblique modes ($\theta\neq0°$) the four regions still exist and only the boundaries, as defined by the $c_\pm$ curves in the phase-speed–Mach-number plane, are changed from those of the two-dimensional modes. Finally, it is important to note that the sonic speeds are independent of the reaction since the far field is chemically frozen. Thus the classification scheme does not depend on the reaction model used.

In all of the stability calculations reported below, we take $D=e^{Ze}$ as is suggested by the asymptotics of Grosch and Jackson.[17] In addition, we take $\gamma=1.4$, $\mathrm{Pr}=1$, $\mathrm{Sc}_j=1$ with varied β, ϕ, Ze, β_U, β_T, and M. Unless otherwise stated, stability calculations were performed at the downstream locations $x=3$ and 10.

IV. LINEAR STABILITY RESULTS

A comprehensive study of the stability of the reacting compressible mixing layer using the hyperbolic tangent for the velocity profile and the flame sheet approximation for the temperature and mass fraction profiles has been carried out by Jackson and Grosch.[16] Since then, Planche and Reynolds[22] have also carried out stability calculations for the flame sheet model using the compressible boundary-layer equations to calculate the velocity profile. Additionally, Shin and Ferziger[23,24] reexamined the stability problem using a model of finite rate chemistry. In all of these studies it was found that the reaction had important and complex effects on the flow stability but only Jackson and Grosch reported the presence of an absolute instability due to the reaction. Because these authors used different models for the mean velocity and temperature profiles, a quantitative comparison of the stability results between the flame sheet model and the finite rate chemistry model is not possible.

Our primary interest is in the transition from convective to absolute instability in reacting flows and the comparison of the results for the finite rate model to those of the flame sheet model. Therefore, we will not present an exhaustive comparison of the stability results using the finite rate chemistry model as opposed to the flame sheet model, but rather highlight some of the differences in the stability of the flow owing to the use of the two models through comparison of the phase speeds of the neutral modes for both models. In this section we consider only two-dimensional disturbances, thus setting $\theta=0°$.

The phase speeds of the subsonic neutral modes with nonzero wave numbers in region 1 can be found by using the regularity condition (Lees and Lin[25]). Let $S(\eta)$ be defined by

$$S(\eta)\equiv\frac{d}{d\eta}\left(T^{-2}\frac{dU}{d\eta}\right). \tag{27}$$

Then if a neutral mode exists with $\alpha\neq0$ in region 1, the phase speed will be given by $c_N=U(\eta_c)$, where η_c is a root of S. The corresponding neutral wave number, α_N, must be determined numerically. In addition to the neutral modes with $\alpha_N\neq0$ there may exist neutral modes having zero wave number. The phase speed of such modes does not satisfy (27) but can be found by an asymptotic analysis of (18) in the limit $\alpha\to0$. The result of this analysis is, for $M=\beta_U=0$,

Reuse of AIP Publishing content is subject to the terms at: https://publishing.aip.org/authors/rights-and-permissions. Download to IP: 128.82.15.135 On: Sun, 28 Aug 2016 19:44:02

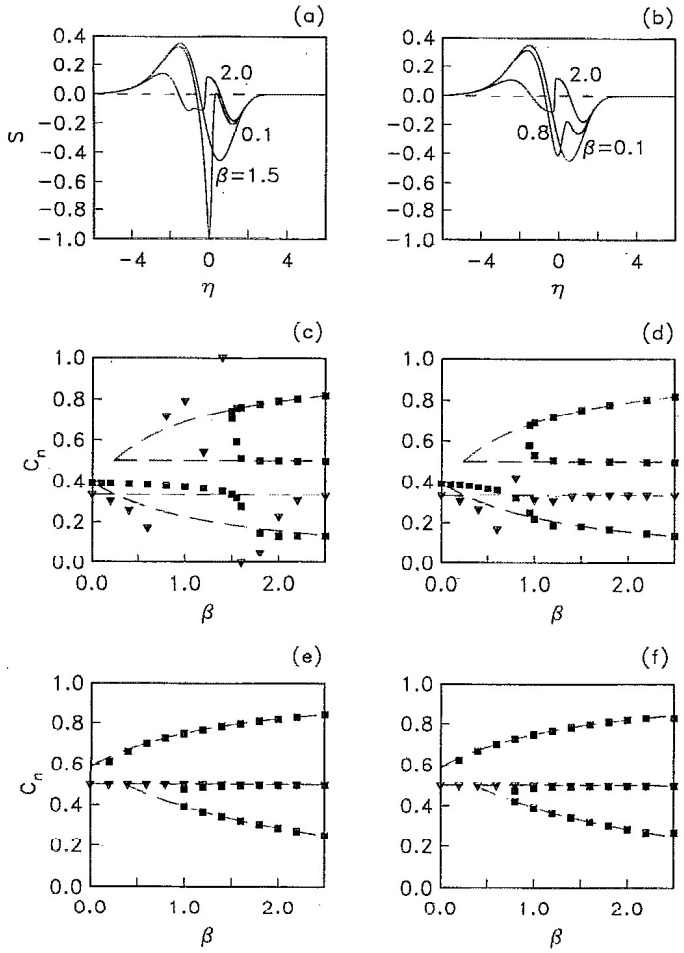

FIG. 2. Plot of S vs η for various values of β with $\beta_U=0$, $\beta_T=0.5$, $\phi=1$, Ze=20, $M=0$ at (a) $x=3$ and (b) $x=10$. Plot of neutral phase speeds versus β with $\beta_T=0.5$ at (c) $x=3$ and (d) $x=10$, and with $\beta_T=1$ at (e) $x=3$ and (f) $x=10$ for the same parameters as (a) and (b). Here - - - in (c)–(f) denotes the neutral phase speeds corresponding to the flame sheet model. The disturbances are two dimensional with $\theta=0°$.

$$c_N=\frac{1+ie^{B/2}}{1+e^{B}},$$
$$B=\int_{-\infty}^{\infty}\frac{(F_1+F_2)T'+\beta(F_1F_2)'}{(F_1+F_2)T-\beta(\mathrm{Ze}-1)F_1F_2T'}\,d\eta. \tag{28}$$

In the nonreactive case ($\beta=0$) (28) reduces to

$$c_N=\frac{\beta_T+i\sqrt{\beta_T}}{\beta_T+1}, \tag{29}$$

which shows that the neutral phase speed is complex for $\alpha_N=0$.

Figures 2(a) and 2(b) are plots of S vs η for various values of the heat release parameter, β, using the finite rate model. The slow stream has a speed $\beta_U=0$ and temperature $\beta_T=0.5$. The equivalence ratio $\phi=1$, with Ze=20 and $M=0$. The results shown in Fig. 2(a) were obtained using the temperature distribution at $x=3$, while those of Fig. 2(b) were obtained using the temperature distribution at $x=10$. As one can see from examination of these figures, the rate of heat release has a significant effect not only on the number of roots of S, but also on their values. When the heat release parameter is small ($\beta=0.1$), there is a single root of S with η_c close to zero at both $x=3$ and 10. With $\beta\approx1.5$ there are three roots of S at $x=3$. One root is located near $\eta_c=-1.5$, while the other two are a double root with η_c just greater than zero. A further increase in β to 2 results in a shift of the first root to more negative values of η and a splitting of the double root into two distinct roots, one close to zero and the other near $\eta=1$. Qualitatively similar behavior is shown in Fig. 2(b) at $x=10$.

The corresponding neutral phase speeds (c_N) (indicated by boxes) obtained from the roots of S are shown in Figs. 2(c) at $x=3$ and 2(d) at $x=10$ for $\beta_T=0.5$ (the slow stream is cool), and Figs. 2(e) at $x=3$ and 2(f) at $x=10$ for $\beta_T=1$ (both streams are at the same temperature). These are shown as functions of the heat release parameter β with the values of the other parameters given above. The real part of the neutral phase speeds for the $\alpha_N=0$ mode, found from (28), is shown in these figures by inverted triangles. The flame sheet model results, shown as dashed lines in these figures, use the Lock velocity profile as required for consistency in comparison with the results using the finite rate chemistry model; thus, they are slightly different from those reported by Jackson and Grosch[16] where a hyperbolic tangent velocity profile was used.

In the nonreactive case ($\beta=0$), there are two neutral modes with different phase speeds which coincide at $\beta_T=0.577\,53$ (Jackson and Grosch[19]). With $\beta_T=0.5$ these neutral modes of the nonreacting flow are slow modes since they have phase speeds less than 0.5 [see Figs. 2(c) and 2(d)]. One of these neutral modes has a phase speed determined by a root of S given by $c_N=0.391\,344$, and the other member of this pair has a phase speed determined by (29) with the value $c_N=(1+i\sqrt{2})/3$. With $\beta_T=1$, these neutral modes are fast modes since they have phase speeds greater than 0.5 [see Figs. 2(e) and 2(f)]. Again, one of these has a phase speed determined by a root of S which is $c_N=0.587\,270$, and the other member of this pair has a phase speed determined by (29) with the value $c_N=(1+i)/2$.

When heat release is included ($\beta>0$) and the flame sheet model is used [denoted by the dashed lines of Figs. 2(c)–2(f), there are, in general, four neutral modes: two are found from the Lees and Lin condition (27), called modes 1 and 2; one is found from the zero wave-number asymptotics (29), called mode 3; and the remaining one, mode 4, is a mode with phase speed $c_N=U(\eta_f)$. The corresponding wave number for this last case needs to be determined in the numerical limit as one approaches the neutral mode through the unstable modes. Of the two neutral modes found from (27), only one (mode 1) exists at $\beta=0$. Mode 1 is a slow mode for $\beta_T<0.577\,53$ and its phase speed is a decreasing function of β [Figs. 2(c) and 2(d)] while for $\beta_T>0.577\,53$, mode 1 is a fast mode whose phase speed is an increasing function of β [Figs. 2(e) and 2(f)]. Mode 2 only exists for $\beta>0$ and shows the opposite behavior of mode 1. The third neutral mode, that with

Reuse of AIP Publishing content is subject to the terms at: https://publishing.aip.org/authors/rights-and-permissions. Download to IP: 128.82.15.135 On: Sun, 28 Aug 2016 19:44:02

$\alpha_N=0$, exists at $\beta=0$ and has a phase speed which is constant for all values of the heat release parameter, β. Finally, the fourth neutral mode appears at the same value of β as the second mode, has a phase speed which is equal to $U(\eta_f)$, and is independent of β. When both streams have the same temperature, $\beta_T=1$, the phase speeds of the third and fourth modes are equal. These neutral curves separate stable from unstable regions with an unstable region lying between modes 1 and 3 (called the slow branch) and another between modes 2 and 4 (called the fast branch).

As with the flame sheet model, there are also four neutral modes when using the finite rate chemistry model. The phase speeds of modes 1, 2, and 4 are determined from the Lees and Lin condition (27), and the third neutral mode is again the zero wave-number mode with phase speed determined from (28). The reason the fourth mode of the flame sheet model is not determined from (27) is that the Lees and Lin condition fails to hold because S is discontinuous and the derivatives of the eigenfunctions become discontinuous at the flame sheet position. For the finite rate chemistry model, the phase speed of the fourth neutral mode approaches that given by mode 4 of the flame sheet model, i.e., $c_N=U(\eta_f)$, as x increases. The phase speeds of the neutral modes 1, 2, and 4 are indicated by boxes in Figs. 2(c)–2(e), and the phase speed of the third neutral mode is indicated by inverted triangles. Unlike the flame sheet model, the neutral phase speeds for modes 3 and 4 are functions of the heat release parameter β and the downstream position x.

The value of the phase speeds of all four neutral modes will depend critically on whether the x location is upstream or downstream of ignition. In the region of ignition, the temperature and mass fraction fields vary rapidly with position and consequently the parallel flow approximation no longer holds. If x is sufficiently downstream of the ignition point, neutral modes 2 and 4 are present. At $x=3$ and with $\beta_T=0.5$ [Fig. 2(c)] the phase speeds of neutral mode 3 show large variations between $0.5<\beta<2$. This is to be expected because ignition occurs in this region and the parallel flow assumption fails. As β is increased past 2, the phase speeds of all four neutral modes approach the phase speeds predicted by the flame sheet model. Similar behavior is shown in Fig. 2(d) at $x=10$. The variations in the real part of the phase speeds of the $\alpha_N=0$ neutral mode appear smaller than at $x=3$ which is consistent with (5b) since the source term is proportional to $x\,\beta$ and thus at larger x the ignition region extends over a smaller range of β. All of the phase speeds which were determined from (27) and (28) have been confirmed by full numerical stability calculations.

V. ABSOLUTE–CONVECTIVE INSTABILITY

In the stability problem, the eigenvalue is a zero of the characteristic equation relating the wave number α and the frequency ω at fixed Mach number. Since $\alpha(\omega)$ has a square root branch point singularity at a zero of the complex group velocity $d\omega/d\alpha$ (Gaster[10]), transition from convective to absolute instability occurs when the zero lies on the real ω axis. We therefore choose ω to be real, α to be complex, and carry out a numerical search for a zero of $d\omega/d\alpha$. In these calculations, we take $\gamma=1.4$, $\mathrm{Pr}=1$, $\mathrm{Sc}_j=1$, and vary β, ϕ, Ze, β_U, β_T, and M. Unless otherwise stated, Ze=20, $M=0$, and $\phi=1$ in all of the calculations reported below. Finally, we note that for spatial stability it was shown by Jackson and Grosch[16] that the fast branch is convectively unstable for all β, while the slow branch undergoes a transition from convective to absolute instability. Hence, all results shown in this section are for the slow branch. We first present results for two-dimensional disturbances ($\theta=0°$) and then for oblique waves.

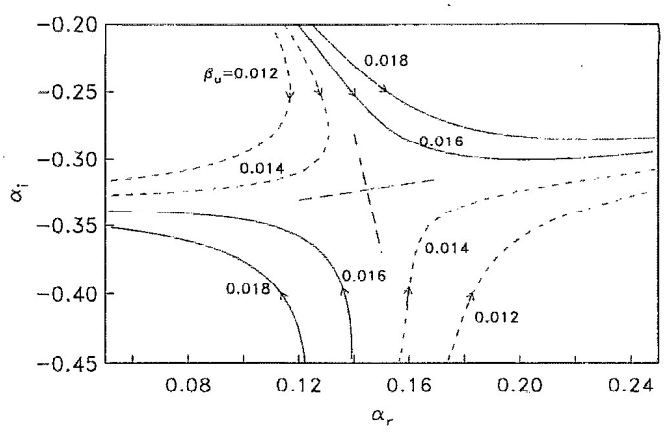

FIG. 3. Plot of α_i vs α_r for various values of β_U at $x=10$ showing the saddle point. Here $\beta=2$, $\phi=1$, $\beta_T=0.5$, Ze=20, and $M=0$. The disturbances are two dimensional with $\theta=0°$.

A plot of α_i vs α_r at $x=10$ as the real frequency ω varies continuously is shown in Fig. 3 with $\beta=2$, $\beta_T=0.5$, $\theta=0°$, and various values of β_U. There is a saddle point for the speed of the slow stream, β_U, between 0.014 and 0.016 which is the same qualitative behavior as first observed with the flame sheet model[16] and shows the presence of a square root branch point singularity due to a transition from convective to absolute instability. For the flame sheet model, this transition from convective to absolute instability occurs at a fixed β_U independent of x. For the finite rate chemistry model, the transition value of β_U is dependent on the downstream position x, and its variation is shown in Fig. 4 for $\beta=2$ and $\beta_T=0.5$. The region below the curve designates conditions in which the flow is absolutely unstable and the region above the curve designates conditions where the flow is convectively unstable. For all non-negative β_U, the flow is convectively unstable up to $x\approx 1.9$, which is just beyond the ignition point. Once ignition has occurred, there is a range of non-negative β_U in which the flow is absolutely unstable. As the flow field evolves downstream, the range of β_U in which there is an absolute instability decreases and asymptotes to that predicted by the flame sheet model given by the dashed line. For the parameters of this calculation, the flow will always exhibit an absolute instability if $0\leqslant\beta_U\leqslant 0.015$ and even up to about 0.038 near the ignition point. The slow moving stream must be nearly stationary if the flow is to be absolutely unstable. This is broadly consistent with previous studies

Reuse of AIP Publishing content is subject to the terms at: https://publishing.aip.org/authors/rights-and-permissions. Download to IP: 128.82.15.135 On: Sun, 28 Aug 2016 19:44:02

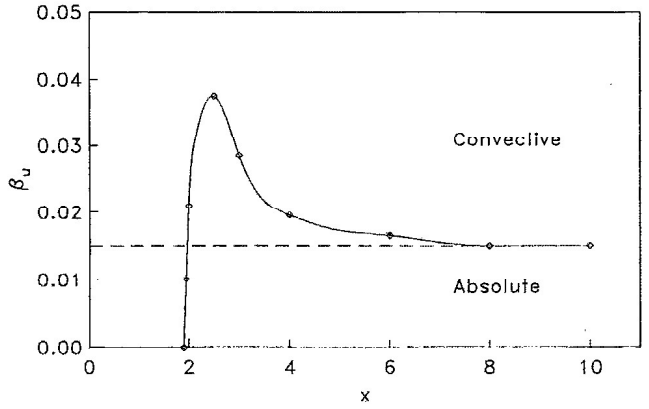

FIG. 4. Transition value of β_U from absolute to convective instability as a function of the downstream coordinate x for $\beta=2$, $\phi=1$, $\beta_T=0.5$, Ze $=20$, and $M=0$. Here - - - denotes the value given by the flame sheet model. The disturbances are two dimensional with $\theta=0°$.

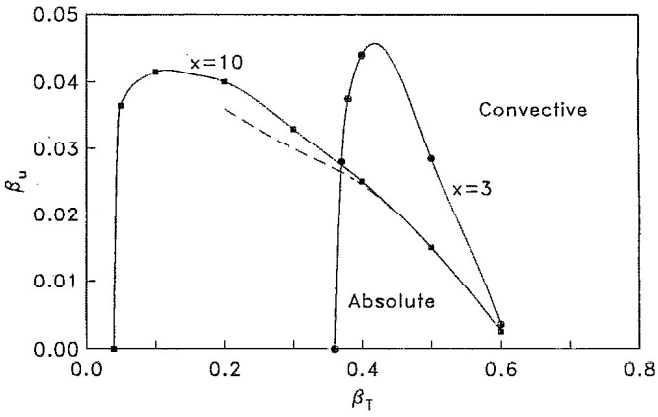

FIG. 6. Transition value of β_U from absolute to convective instability as a function of β_T for $\phi=1$, $\beta=2$, Ze$=20$, and $M=0$ at $x=3$ and 10. Here - - - denotes the value given by the flame sheet model. The disturbances are two dimensional with $\theta=0°$.

where an absolute instability was only found if the streams were moving in opposite directions.

The boundary between regions of convective and absolute instability in the parameter space is mapped out by a systematic set of calculations at two fixed locations: $x=3$ and 10. These results are presented in Figs. 5–10 for two-dimensional disturbances with $\theta=0°$. For the results shown in Figs. 5–8 the Mach number is zero. The Mach number is varied for the results shown in Figs. 9 and 10. The results presented in Figs. 11 and 12 show the boundary of the region of absolute instability in the β_U–Mach-number plane for oblique waves with $\theta\neq0°$.

In Fig. 5 we show the locus of the branch point position in the β_U-β plane for $\beta_T=0.5$. The region to the left of each curve is that of convective instability and that to the right the region of absolute instability. At $x=3$ the flow can become absolutely unstable for the heat release parameter $\beta\geqslant1.55$ if the speed of the slow stream β_U is sufficiently small. On the other hand, at $x=10$ the transition from convective to absolute instability first occurs at $\beta\approx1.3$ with $\beta_U=0$. For $\beta>1.3$ the flow can be absolutely unstable for some range of positive β_U. Also at $x=10$, the flame sheet model results (dashed) are in excellent agreement with those obtained using the finite rate chemistry model. Even at $x=3$, the finite rate chemistry model results asymptote to the flame sheet model results as β is increased. In Fig. 6, the effect of the temperature ratio β_T on the transition value of the speed at $-\infty$, β_U, at a value of the heat release parameter of $\beta=2$ is shown. The region below each curve is that of absolute instability. At this value of β the flow is always convectively unstable for $\beta_T>0.62$. At both $x=3$ and 10 there is a range of cooling of the stream at $-\infty$ for which the flow becomes absolutely unstable provided that β_U is sufficiently close to zero. The range of β_T for which absolute instability can occur is smaller at $x=3$ than at $x=10$. Figure 7 is a plot of the transition value of β_U versus the Zeldovich number at $\beta=2$ and $\beta_T=0.5$. Decreasing values of Ze result in a decrease in the transition value of

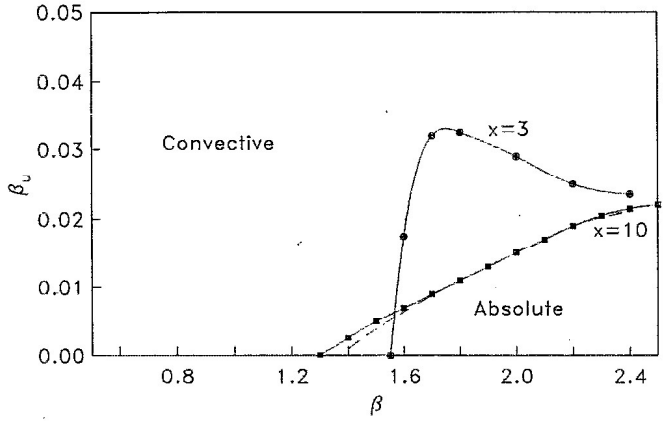

FIG. 5. Transition value of β_U from absolute to convective instability as a function of β for $\phi=1$, $\beta_T=0.5$, Ze$=20$, and $M=0$ at $x=3$ and 10. Here - - - denotes the value given by the flame sheet model. The disturbances are two dimensional with $\theta=0°$.

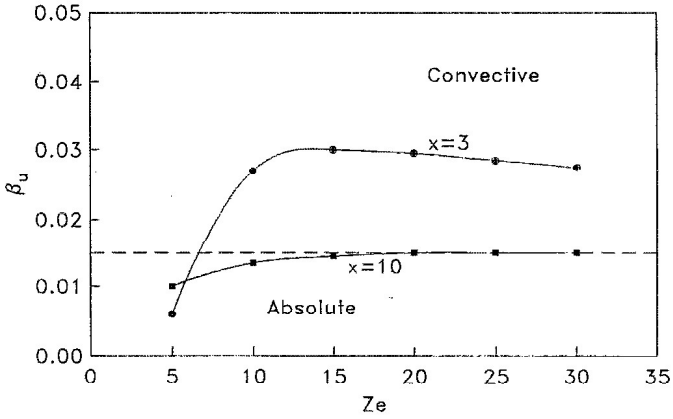

FIG. 7. Transition value of β_U from absolute to convective instability as a function of Ze for $\phi=1$, $\beta=2$, $\beta_T=0.5$, and $M=0$ at $x=3$ and 10. Here - - - denotes the value given by the flame sheet model. The disturbances are two dimensional with $\theta=0°$.

Reuse of AIP Publishing content is subject to the terms at: https://publishing.aip.org/authors/rights-and-permissions. Download to IP: 128.82.15.135 On: Sun, 28 Aug 2016 19:44:02

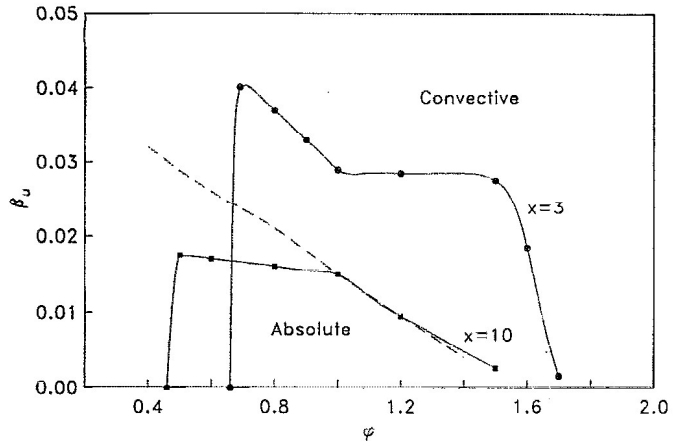

FIG. 8. Transition value of β_U from absolute to convective instability as a function of ϕ for $\beta=2$, $\beta_T=0.5$, Ze=20, and $M=0$ at $x=3$ and 10. Here – – – denotes the value given by the flame sheet model. The disturbances are two dimensional with $\theta=0°$.

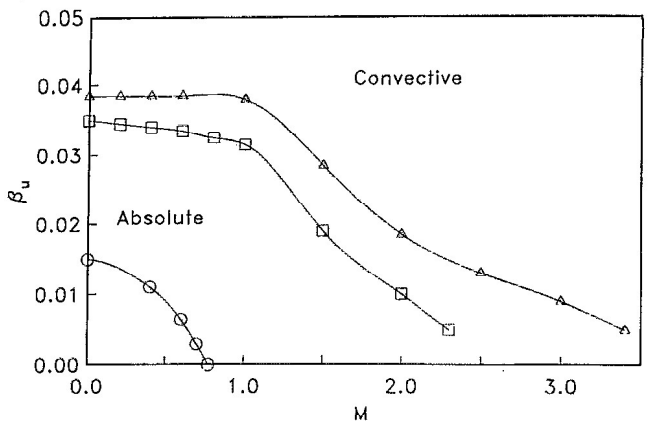

FIG. 10. Transition value of β_U from absolute to convective instability for the flame sheet model as a function of M with $\phi=1$. Results are shown for –○–:$\beta_T=0.5$ and $\beta=2$; –□–:$\beta_T=0.15$ and $\beta=2$; and –△–:$\beta_T=0.15$ and $\beta=4$. The disturbances are two dimensional with $\theta=0°$.

β_U. At $x=3$ the transition from convective to absolute instability does not occur for values of Ze less than about 4. Also at the same x there is a substantial difference between the finite rate chemistry model results and that of the flame sheet model (dashed) even at large Ze. On the other hand, at $x=10$ it is apparent that for Ze larger than about 10 there is essentially no effect of increasing Ze on the transition value which is nearly the same as that calculated from the flame sheet model. Figure 8 is a plot of the transition value of β_U versus the equivalence ratio at $\beta=2$ and $\beta_T=0.5$. For fuel lean mixtures (i.e., $\phi<1$) the region of absolute instability is slightly enhanced. For fuel rich mixtures there is a substantial decrease in the transition value of β_U, and beyond $\phi\approx1.7$, the flow is always convectively unstable.

The effect of increasing the Mach number on the transition value of β_U with a fixed heat release, $\beta=2$, equivalence ratio, $\phi=1$, and temperature at $-\infty$, $\beta_T=0.5$, is shown in Fig. 9. Increasing the Mach number decreases the region of absolute instability until it completely disappears at $M\approx0.8$. At any Mach number less than 0.8 the range of β_U over which the flow is absolutely unstable decreases with increasing downstream distance. The effect of varying the temperature at $-\infty$, β_T, and the heat release parameter β, on the boundary between the regions of convective and absolute instability in the β_U-M plane is shown in Fig. 10. With β fixed, decreasing β_T, that is, cooling the flow at $-\infty$, results in an increase in the range of β_U for which the flow is absolutely unstable. Similarly, increasing the heat release parameter, β, with fixed temperature at $-\infty$ also increases the range of β_U over which the flow is absolutely unstable. Although the range of β_U over which the flow is absolutely unstable is largest for subsonic flow, sufficient cooling at $-\infty$ and/or heat release can cause an absolute instability for supersonic mixing layers.

Finally, in Figs. 11 and 12 we show how having obliquely traveling disturbances affects the convective/absolute instability transition. The results presented in Fig. 11 show that increasing the angle of propagation with re-

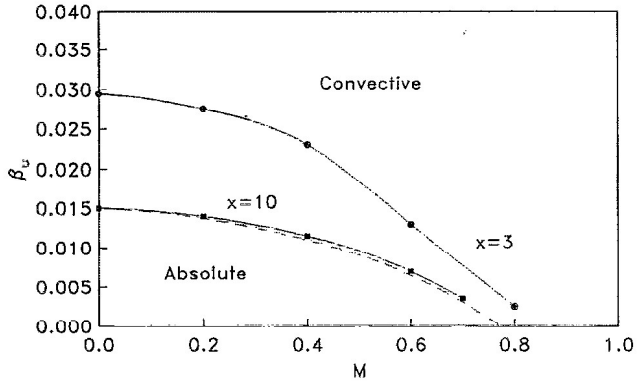

FIG. 9. Transition value of β_U from absolute to convective instability as a function of M for $\phi=1$, $\beta=2$, $\beta_T=0.5$, and Ze=20 at $x=3$ and 10. Here – – – denotes the value given by the flame sheet model. The disturbances are two dimensional with $\theta=0°$.

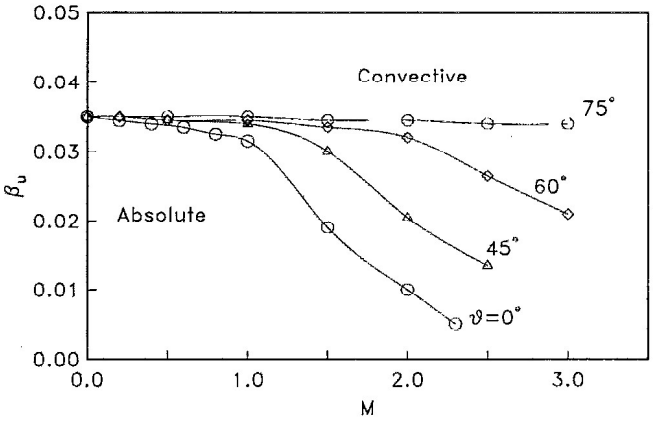

FIG. 11. Transition value of β_U from absolute to convective instability for the flame sheet model as a function of M with $\phi=1$, $\beta=2$, and $\beta_T=0.15$ for two-dimensional and oblique disturbances with $\theta=0°$, 45°, 60°, and 75°.

Reuse of AIP Publishing content is subject to the terms at: https://publishing.aip.org/authors/rights-and-permissions. Download to IP: 128.82.15.135 On: Sun, 28 Aug 2016 19:44:02

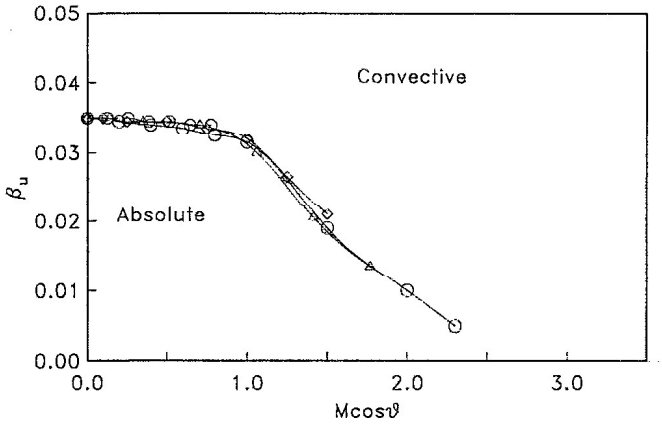

FIG. 12. Transition value of β_U from absolute to convective instability for the flame sheet model as a function of $M\cos\theta$ for $\phi=1$, $\beta=2$, $\beta_T=0.15$, and $Ze=20$ at $x=10$ for two-dimensional and oblique disturbances with $\theta=0°$, 45°, 60°, and 75°.

spect to the mean flow direction, θ, increases the range of β_U over which the reacting flow is absolutely unstable, at least over the parameter ranges examined in this study. This effect seems to be a purely kinematic one in that the wave propagating at an oblique angle relative to the mean flow direction "sees" a flow with a lower Mach number. This is evident from Fig. 12 where the data of Fig. 11 are plotted versus an effective Mach number, $M\cos\theta$, for the oblique disturbances. This rescaling collapses all of the curves of Fig. 11 onto essentially a single curve, corresponding that for $\theta=0°$.

The results presented in Figs. 4–12 give a rather complex picture of the convective/absolute instability transition in the reacting mixing layer. The complexity is in part due to the fact that the reacting mean flow is governed by a large number of parameters. However, despite this, a overall interpretation of these results can be suggested which leads to a better understanding of the convective/absolute transition in both reacting and nonreacting flows.

Previous studies of the convective/absolute instability transition in nonreacting subsonic compressible mixing layers[13–15] have shown them to be convectively unstable unless there was an appreciable backflow. Thus the velocity shear must be sufficiently large for the mixing layer to be absolutely unstable. With the Mach number less than one, the temperature gradient within the layer does not appear to have a major effect on the transition to absolute instability of a nonreacting compressible mixing layer. In the case of a *reacting* mixing layer the magnitude of the required velocity shear is reduced so that the flow with a non-negative β_U can be absolutely unstable. This suggests that the increased temperature gradient within the layer due to the reaction can trigger an absolute instability without backflow, i.e., with a non-negative critical value of β_U. All of the results presented in Figs. 5–12 are consistent with this conclusion which is explored in more detail below.

Because of the approximations used in this study the velocity profile (thus the shear across the layer) is dependent on only one parameter, β_U. (This is an advantage of using the simple property variations as discussed above; the velocity and temperature gradients can be varied independently which is not possible for more complex thermodynamic models of the fluid). As mentioned above, $\beta_U \geqslant 0$ because solutions to (5a) for the velocity field do not exist with backflow at $-\infty$. The results presented here show that the flow upstream of ignition is always convectively unstable. We could have carried out stability calculations within the ignition region but the results would be of rather dubious validity because the large streamwise variation in temperature which occurs within a small distance in the ignition region violates the quasiparallel flow assumption. However, just downstream of ignition our results show that the flow can be absolutely unstable over a range of non-negative β_U, at least for some range of Mach numbers. Thus the temperature and mass fraction distributions across the *reacting* layer must have a major effect on the convective/absolute instability transition. In particular, the presence of a large temperature gradient due to the reaction in the mixing layer appears to cause a convective/absolute transition. We further note that the combustion zone evolves to a flame sheet with increasing distance downstream of ignition[17] and that the results of Figs. 5–12 indicate that the trends in the convective/absolute transition as the flow parameters are varied are reasonably well predicted using the flame sheet model. This suggests that the results of the flame sheet model [described by Eqs. (7)–(10)] are not spurious results owing to the discontinuity of derivatives at the flame sheet, but are real effects of a concentrated addition of heat. The agreement of the finite rate and flame sheet results indicates that we can use the flame sheet model to investigate the trends.

The results of Figs. 9–12 show that, whatever the values of the other parameters, this flow will be convectively, rather than absolutely, unstable at sufficiently large Mach number. From Eqs. (7b) and (8b) it is clear that, for any β and ϕ, if M is large enough the temperature distribution in the layer will be approximated by that of a nonreacting flow which requires a negative β_U for an absolute instability. Thus large Mach numbers cause the flow to be convectively, rather than absolutely, unstable. From Figs. 5 and 10 in particular, cooling the slow stream (decreasing β_T) and increasing the heat release (increasing β) both cause an increase in the range of β_U and Mach number over which an absolute instability exists. An increase in β increases the magnitude of the temperature gradient in $\eta<\eta_f$ and decreases it in $\eta>\eta_f$. However, the magnitude of the temperature gradient on both sides of the flame is increased by a decrease in β_T. This suggests that it is the magnitude of the temperature gradient induced by the flame which must be large for the absolute instability to occur.

Finally, one can see why a very rich or very lean mixture inhibits absolute instability. If the flow is very fuel rich, $\phi \gg 1$, Eq. (9) yields $U_f \approx \beta_U$ so $\eta_f \to -\infty$ and from Eq. (10) $T_f \approx \beta_T$. On the other hand if the flow is very fuel lean, $\phi \to 0$, Eq. (9) shows $U_f \approx 1$ and $\eta_f \to +\infty$. This gives, from Eq. (10), $T_f \approx 1+\beta$. In both cases there is a

Reuse of AIP Publishing content is subject to the terms at: https://publishing.aip.org/authors/rights-and-permissions. Download to IP: 128.82.15.135 On: Sun, 28 Aug 2016 19:44:02

distinct flame (the flame sheet) but it occurs far away from the center of the mixing layer. Since $\partial T/\partial \eta$ is proportional to $\partial U/\partial \eta$, which is very small outside of center of the layer, the temperature gradient due to the flame is very small; thus absolute instability is not present. These considerations suggest that a slightly lean mixture will enhance absolute instability while a very lean or very rich mixture will inhibit absolute instability as is shown in Fig. 8.

VI. WAVE PACKETS

In the previous section we found that the flame sheet model can provide excellent predictions on the transition values provided one is downstream of ignition and Zeldovich numbers are greater than about 10. Therefore, in calculating the wave packets we use the flame sheet model described in Sec. II. The equation governing the stability of this flow is (18) with $K_1=K_2=1$, valid on either side of the flame sheet. To illustrate the dynamics of the instability, contrasting the cases of convective instability and absolute instability, we present selected results for $\beta_U=0$, $\beta_T=0.5$, and $\phi=1$ and vary β and M. We take $\theta=0°$ in this section and thus consider only two-dimensional wave packets.

Figures 2(c) and 2(d) show the variation of the phase speeds of the neutral modes as a function of β. As discussed in Sec. IV there can be both fast and slow neutral branches and hence both fast and slow unstable modes. The fast branch is convectively unstable for all β, while the slow branch may undergo a transition from convective to absolute instability. This behavior is illustrated in Fig. 13 where we plot the spatial growth rates of both the fast and slow branches as a function of ω for several values of β. The fast branch shows regular behavior as β increases, with the maximum value of the growth rate first increasing and then decreasing slightly. In addition, the range of unstable frequencies increases with increasing β. On the other hand, for the slow branch the spatial growth rate forms a cusp as β approaches 1.38, indicating the transition from convective to absolute instability. This transition can also occur at fixed β as one of the other parameters is varied; for example, Fig. 3 shows the saddle point in the complex α plane which occurs as β_U is varied with $\beta=2$. For temporal stability, the growth rates of both the fast and slow branches, shown in Fig. 14, have regular behavior as β is increased and therefore do not indicate a transition from convective to absolute instability even though such a transition occurs at the same value of β. This difference in the behavior of spatial stability as opposed to temporal stability was first noted by Gaster.[10]

A complementary approach to investigate the transition from convective to absolute instability is to examine the response, $I(x,t)$, of the flow to an impulse in space and time (see Huerre and Monkewitz[12] and the references cited therein). The impulse gives rise to a wave packet in the (x,t) plane. The real part of I is the wave packet and its absolute value is the envelope. An asymptotic expansion of the impulse response for large time can be determined by

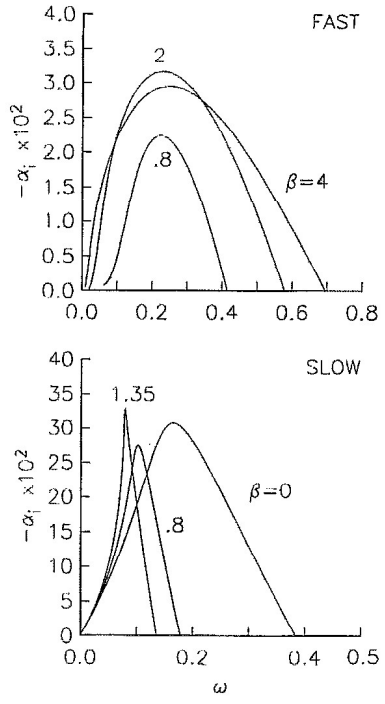

FIG. 13. Plot of the growth rates of the spatial stability problem for the fast and slow modes of the flame sheet model as a function of ω for various values of β. Here $M=0$, $\beta_T=0.5$, $\beta_U=0$, and $\phi=1$. The disturbances are two dimensional with $\theta=0°$.

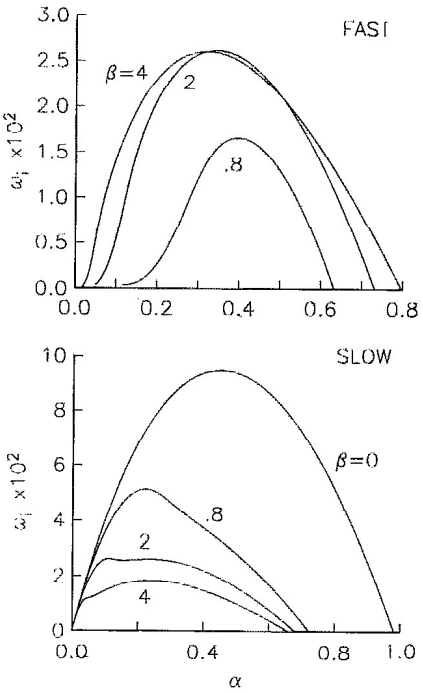

FIG. 14. Plot of the growth rates of the temporal stability problem for the fast and slow modes of the flame sheet model as a function of α for various values of β. Here $M=0$, $\beta_T=0.5$, $\beta_U=0$, and $\phi=1$. The disturbances are two dimensional with $\theta=0°$.

Reuse of AIP Publishing content is subject to the terms at: https://publishing.aip.org/authors/rights-and-permissions. Download to IP: 128.82.15.135 On: Sun, 28 Aug 2016 19:44:02

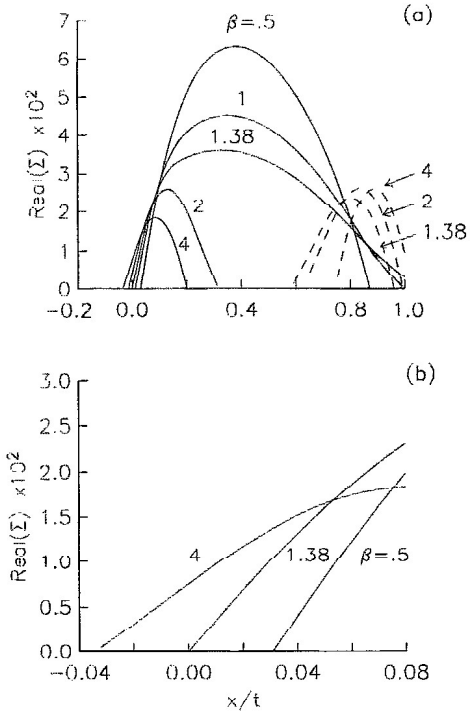

FIG. 15. (a) Plot of the real part of Σ as a function of x/t for various values of β. (b) Enlargement of (a) in the region $-0.04<x/t<0.08$. Here $M=0$, $\beta_T=0.5$, $\beta_U=0$, and $\phi=1$. The disturbances are two dimensional with $\theta=0°$.

the method of steepest descent. The details of this analysis are given by Gaster[11,26] and for what follows we use the leading term in his expansion,

$$I=\left(\frac{2\pi}{(d^2\omega/d\alpha^2)t}\right)^{1/2}_{\alpha=\alpha^*} e^{\Sigma t}[1+O(t^{-1})], \tag{30}$$

where

$$\Sigma=i\left(\alpha^*\frac{x}{t}-\omega(\alpha^*)\right). \tag{31}$$

The value of α^* is found from the requirement that the rays in the wave packet have constant real values of the group velocity, C_g. Thus,

$$C_g=\left(\frac{d\omega}{d\alpha}\right)_{\alpha=\alpha^*}=\frac{x}{t}. \tag{32}$$

The set of $\{\alpha^*,\omega(\alpha^*)\}$ pairs which satisfy (32) are found by choosing a (real) value of x/t and then carrying out an iterative search in the complex α and ω spaces for an α^* which satisfies (32) and also permits the solution of (18) with the appropriate boundary conditions.

There are two, generally distinct, wave packets: the first is made up of the unstable modes of the slow branch, which are absolutely unstable in certain parameter ranges, and the second is made up of the unstable modes of the fast branch which are always convectively unstable. The real part of Σ, the temporal growth rate along the rays, is plotted in Fig. 15 for both the fast and slow unstable branches

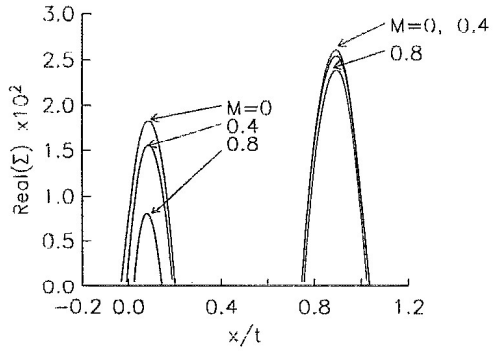

FIG. 16. Plot of the real part of Σ as a function of x/t for various Mach numbers. Here $\beta=4$, $\beta_T=0.5$, $\beta_U=0$, and $\phi=1$. The disturbances are two dimensional with $\theta=0°$.

at $M=0$ for various values of β. As β increases, the maximum of the real part of Σ for the slow branch decreases and the range of x/t for which the real part of Σ is positive decreases. For the fast branch, the maximum growth rate increases by a small amount, and the range of unstable frequencies increases. Figure 15(b) is an enlargement of Fig. 15(a) near $x/t=0$. The real part of Σ goes to zero at x/t slightly above 0.03 for $\beta=0.5$. For $\beta=1.38$, it is zero at $x/t=0$, and for $\beta=4$, it is zero at $x/t\approx-0.035$. The fact that the real part of Σ is positive for a range of negative values of x/t shows that the wave packet is traveling *both* upstream and downstream and therefore that the flow is absolutely unstable. It is important to note that the growth rates in the region of $x/t<0$ are small compared to the maximum growth rate. This shows that the upstream propagating portion of the wave packet grows slowly compared to the downstream propagating part. The effect of increasing the Mach number on the temporal growth rate along the rays is shown in Fig. 16 where the variation of Σ with x/t for $\beta=4$ and various Mach numbers is shown. The temporal growth rates for the fast branch are only slightly affected by the change in M from 0 to 0.8 with a small decrease in the maximum and the range of x/t over which it is positive. There is a much greater effect on the slow branch. The peak value decreases by more than a factor of 2 as M increases to 0.8 and the range of x/t over which this branch is unstable decreases. For $M=0.8$ the slow branch only has a positive growth rate for $x/t>0$ indicating that there is no absolute instability at this Mach number.

The wave packets resulting from the impulse with $M=0$ and $\beta=4$ are shown at (a) $t=100$ and (b) $t=500$ in Fig. 17. In each figure there is a pair of wave packets: one is a fast packet containing the unstable modes of the fast branch and the other a slow packet containing the unstable mode of the slow branch. As the pair evolves in time, they move apart because of the substantial differences in their group velocities. At $t=100$ [Fig. 17(a)] the slow packet is somewhat larger than the fast packet and clearly exists in a region of $x<0$ showing the absolute instability. At $t=500$ [Fig. 17(b)] both packets have grown, spread, and moved apart. The notation, $\times10$, close to the slow packet means that the amplitude of the slow packet, but not that of the

Reuse of AIP Publishing content is subject to the terms at: https://publishing.aip.org/authors/rights-and-permissions. Download to IP: 128.82.15.135 On: Sun, 28 Aug 2016 19:44:02

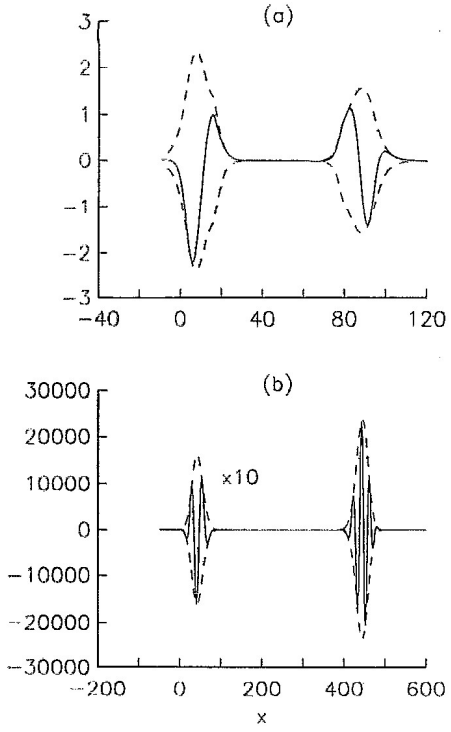

FIG. 17. Plot of the wave packets and envelopes for the fast and slow modes as a function of x at (a) $t=100$ and (b) $t=500$. The slow packet is absolutely unstable and the fast packet convectively unstable. Here $\beta=4$, $M=0$, $\beta_T=0.5$, $\beta_U=0$, and $\phi=1$. The disturbances are two dimensional with $\theta=0°$.

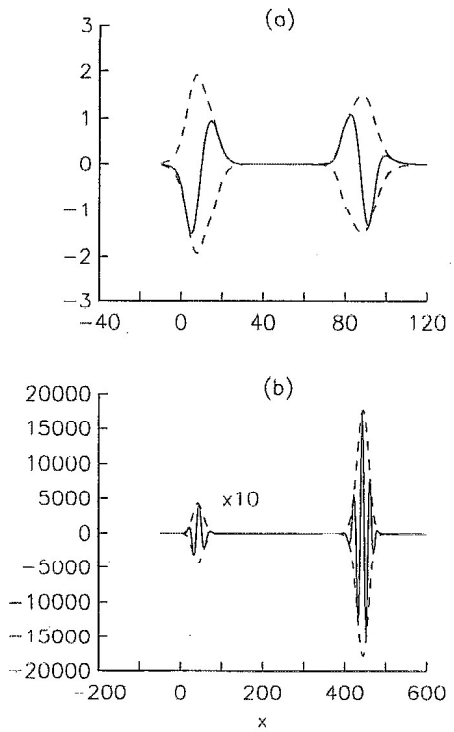

FIG. 18. Plot of the wave packets and envelopes for the fast and slow modes as a function of x at (a) $t=100$ and (b) $t=500$. The slow packet is absolutely unstable and the fast packet convectively unstable. Here $\beta=4$, $M=0.4$, $\beta_T=0.5$, $\beta_U=0$, and $\phi=1$. The disturbances are two dimensional with $\theta=0°$.

fast packet, has been multiplied by a factor of 10 in order that it be visible on this scale. In Fig. 17(b) the fast packet is much larger than the slow packet because of its greater growth rate. The slow wave packet extends into the region $x<0$, but because of the scaling it is difficult to see this on the figure. As time increases, the slow packet will continue to grow, but at a much slower rate than the fast packet, and spread both upstream and downstream. However, the upstream propagation is very slow.

Figure 18 shows the wave packets generated with $\beta=4$, as in Fig. 17, but with $M=0.4$. Both packets have nearly the same group velocity as at $M=0$ but smaller growth rates. Again, the upstream propagation of the slow packet at $t=100$ is visible but is not readily visible at $t=500$ because of the scale. Since there is a substantial decrease in the growth rates of the slow branch relative to those of the fast branch as Mach number increases, the slow packet is much smaller than the fast packet, particularly at $t=500$. With the Mach number increased to 0.8 (Fig. 19), the absolute instability has vanished [the upstream propagation shown in Fig. 19(a) is artificial owing to the relatively small time, for larger time it has completely disappeared consistent with the results of Fig. 16]. The amplitudes of both branches are further decreased because of the increase in the Mach number, with that of the slow branch more so than that of the fast branch. The fast packet at this Mach number is much larger than the slow packet; note the scaling of 500 for the slow packet in this figure. The absolute instability is also absent at higher Mach numbers. The results presented here on the convective–absolute transition have been for $\beta_T=0.5$. Similar results are also found at other values of β_T.

VII. CONCLUSIONS

In this paper we have studied the absolute/convective instabilities of a compressible mixing layer with finite rate chemistry using a one-step, irreversible reaction of Arrhenius type. It is important to note that the similarity solution for the velocity profile does *not* permit reverse flow, and thus all results presented here are for coflowing mixing layers.

It was found that absolute instability occurs for moderate heat release without the introduction of backflow. The effects of the temperature ratio, heat release parameter, Zeldovich number, equivalence ratio, direction of propagation of the disturbances, and the Mach number on the transition value of the velocity ratio were given. It was found that the flame sheet model provides excellent predictions on the transition values provided one is downstream of ignition and Zeldovich numbers are greater than about 10. In particular, with fixed but small velocity ratio, it is possible to induce an absolute instability by increasing the heat release parameter or by decreasing either the equivalence ratio or the temperature ratio. If the slow stream is sufficiently cool and the heat release sufficiently large an absolute instability occurs with the fast stream

Reuse of AIP Publishing content is subject to the terms at: https://publishing.aip.org/authors/rights-and-permissions. Download to IP: 128.82.15.135 On: Sun, 28 Aug 2016 19:44:02

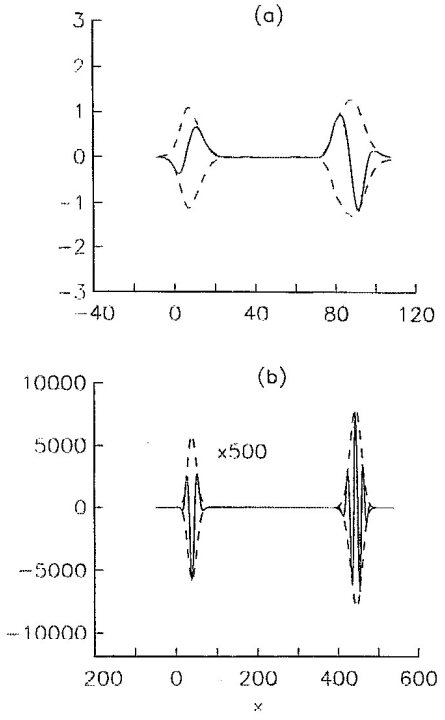

FIG. 19. Plot of the wave packets and envelopes for the fast and slow modes as a function of x at (a) $t=100$ and (b) $t=500$. Both the slow and fast packets are convectively unstable. Here $\beta=4$, $M=0.8$, $\beta_T=0.5$, $\beta_U=0$, and $\phi=1$. The disturbances are two dimensional with $\theta=0°$.

moderately supersonic. For a sufficiently rich mixture the flow will always be convectively unstable. We conclude, on the basis of the results of our calculations and the analysis of Sec. V, that cooling the slow stream (decreasing β_T), using a slightly lean mixture ($\phi<1$), and having a large heat release (large β) will all tend to increase the magnitude of the temperature gradient in the layer and that this causes the flow to undergo a transition from convective to absolute instability. We also showed that the effect of the direction of propagation on the transition from convective to absolute instability is a kinematic one. The flow field sees the effective Mach number ($M\cos\theta$) in the direction of propagation.

Finally, we have shown that wave packet calculations are very useful for displaying the structure of both convectively and absolutely unstable flows. Because there is both a slow and a fast branch of unstable waves an impulse generates a pair of wave packets in both the case of absolute as well as convective instability. In particular, the wave packet calculations have shown that when the reacting shear layer is absolutely unstable it is *weakly* unstable. That is, with increasing Mach number from zero and a fixed rate of heat release, the absolute instability becomes progressively weaker in that the range of negative x/t over which the growth rate is non-negative grows smaller and the growth rate in this region and the speed of the upstream traveling waves also become smaller. Thus a wave packet will grow and spread throughout the entire domain, but it may take a long time for this to happen.

In future work, we plan to carry out numerical simulations of the absolutely unstable mixing layer with finite rate chemistry. This approach is similar to that of Hannemann and Oertel[27] who studied the absolute/convective instabilities of the nonreacting incompressible wake. The object of this will be to examine the effects of the nonparallel mean flow, in particular in the ignition region, and the nonlinearity of the disturbances.

ACKNOWLEDGMENTS

We wish to thank Michael Gaster for helpful discussions and for giving us his wave-tracing code. We thank the referees for helpful comments.

F. Q. H. was supported by an Old Dominion University Summer Faculty Research Fellowship. T. L. J. was supported by AFOSR Contract No. 91-0180. D. G. L. was supported by NSF Grant No. DMS-9007642. C. E. G. was supported by AFOSR Contract No. 91-0250.

[1] T. L. Jackson, "Stability of laminar diffusion flames in compressible mixing layers," in *Major Research Topics in Combustion*, edited by M. Y. Hussaini, A. Kumar, and R. Voigt (Springer-Verlag, Berlin, 1992), pp. 131–161.
[2] H. L. Beach, "Supersonic combustion status and issues," in Ref. 1, pp. 1–20.
[3] J. P. Drummond and H. S. Mukunda, "A numerical study of mixing enhancement in supersonic reacting flow fields," AIAA Paper No. 88-3260, 1988.
[4] G. L. Brown and A. Roshko, "On density effects and large structure in turbulent mixing layers," J. Fluid Mech. **64**, 775 (1974).
[5] N. Chinzei, G. Masuya, T. Komuro, A. Murakami, and D. Kudou, "Spreading of two-stream supersonic turbulent mixing layers," Phys. Fluids **29**, 1345 (1986).
[6] D. Papamoschou and A. Roshko, "Observations of supersonic free-shear layers," AIAA Paper No. 86-0162, 1986.
[7] D. Papamoschou and A. Roshko, "The compressible turbulent shear layer: An experimental study," J. Fluid Mech. **197**, 453 (1988).
[8] N. T. Clemens, "An experimental investigation of scalar mixing in supersonic turbulent shear layers," HTGL Report No. T-274, Department of Mechanical Engineering, Stanford University, 1992.
[9] R. J. Briggs, *Electron–Stream Interaction with Plasmas*, Research Monograph No. 29 (MIT Press, Cambridge, MA, 1964).
[10] M. Gaster, "Growth of disturbances in both space and time," Phys. Fluids **11**, 723 (1968).
[11] M. Gaster, "Propagation of linear wave packets in laminar boundary layers," AIAA J. **19**, 419 (1981).
[12] P. Huerre and P. A. Monkewitz, "Local and global instabilities in spatially developing flows," Annu. Rev. Fluid Mech. **22**, 473 (1990).
[13] P. Huerre and P. A. Monkewitz, "Absolute and convective instabilities in free shear layers," J. Fluid Mech. **159**, 151 (1985).
[14] S. Pavithran and L. G. Redekopp, "The absolute–convective transition in subsonic mixing layers," Phys. Fluids A **1**, 1736 (1989).
[15] T. L. Jackson and C. E. Grosch, "Absolute/convective instabilities and the convective Mach number in a compressible mixing layer," Phys. Fluids A **2**, 949 (1990).
[16] T. L. Jackson and C. E. Grosch, "Inviscid spatial stability of a compressible mixing layer. Part 2. The flame sheet model," J. Fluid Mech. **217**, 391 (1990).
[17] C. E. Grosch and T. L. Jackson, "Ignition and structure of a laminar diffusion flame in a compressible mixing layer with finite rate chemistry," Phys. Fluids A **3**, 3087 (1991).
[18] J. D. Anderson, *Hypersonic and High Temperature Gas Dynamics* (McGraw-Hill, New York, 1989).
[19] T. L. Jackson and C. E. Grosch, "Inviscid spatial stability of a compressible mixing layer. Part 3. Effect of thermodynamics," J. Fluid Mech. **224**, 159 (1991).
[20] A. F. Ghoniem and G. Heidarinejad, "Effect of Damkohler number on

Reuse of AIP Publishing content is subject to the terms at: https://publishing.aip.org/authors/rights-and-permissions. Download to IP: 128.82.15.135 On: Sun, 28 Aug 2016 19:44:02

the reactive zone structure in a shear layer," Combust. Flame **83**, 1 (1991).
[21]T. L. Jackson and C. E. Grosch, "Inviscid spatial stability of a compressible mixing layer," J. Fluid Mech. **208**, 609 (1989).
[22]O. H. Planche and W. C. Reynolds, "Compressibility effect on the supersonic reacting mixing layer," AIAA Paper No. 91-0739, 1991 (presented at the 29th Aerospace Sciences Meeting, Reno, Nevada).
[23]D. Shin and J. Ferziger, "Linear stability of the reacting mixing layer," AIAA Paper No. 90-0268, 1990 (presented at the 28th Aerospace Sciences Meeting, Reno, Nevada).
[24]D. S. Shin and J. H. Ferziger, "Stability of compressible reacting mixing layer," AIAA Paper No. 91-0372, 1991 (presented at the 29th Aerospace Sciences Meeting, Reno, Nevada).
[25]L. Lees and C. C. Lin, "Investigation of the stability of the laminar boundary layer in a compressible fluid," NACA Tech. Note 1115 (1946).
[26]M. Gaster, "Estimates of the errors incurred in various asymptotic representations of wave packets," J. Fluid Mech. **121**, 365 (1982).
[27]K. Hannemann and H. Oertel, "Numerical simulation of the absolutely and convectively unstable wake," J. Fluid Mech. **199**, 55 (1989).

Reuse of AIP Publishing content is subject to the terms at: https://publishing.aip.org/authors/rights-and-permissions. Download to IP: 128.82.15.135 On: Sun, 28 Aug 2016 19:44:02